NeuroImage 211 (2020) 116612

Contents lists available at ScienceDirect

NeuroImage

journal homepage: www.elsevier.com/locate/neuroimage

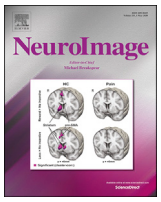

Space-independent community and hub structure of functional brain networks

Farnaz Zamani Esfahlani [a], Maxwell A. Bertolero [b], Danielle S. Bassett [b,c,d,e,f], Richard F. Betzel [a,g,h,i,*]

[a] Department of Psychological and Brain Sciences, Indiana University, Bloomington, IN, 47405, USA
[b] Department of Bioengineering, University of Pennsylvania, Philadelphia, PA, 19141, USA
[c] Department of Electrical & Systems Engineering, University of Pennsylvania, Philadelphia, PA, 19141, USA
[d] Department of Neurology, University of Pennsylvania, Philadelphia, PA, 19141, USA
[e] Department of Psychiatry, University of Pennsylvania, Philadelphia, PA, 19141, USA
[f] Department of Physics & Astronomy, University of Pennsylvania, Philadelphia, PA, 19141, USA
[g] Cognitive Science Program, Indiana University, Bloomington, IN, 47405, USA
[h] Program in Neuroscience, Indiana University, Bloomington, IN, 47405, USA
[i] Network Science Institute, Indiana University, Bloomington, IN, 47405, USA

A B S T R A C T

Coordinated brain activity reflects underlying cognitive processes and can be modeled as a network of inter-regional functional connections. The most costly connections in the network are long-distance correlations that, in the absence of underlying structural connections, are maintained by sustained energetic inputs. Here, we present a spatial modeling approach that amplifies contributions made by long-distance functional connections to whole-brain network architecture, while simultaneously suppressing contributions made by short-range connections. We use this method to characterize the long-distance architecture of functional networks and to identify aspects of community and hub structure that are driven by long-distance correlations and that, we argue, are of greater functional significance. We find that based only on patterns of long-distance connectivity, primary sensory cortices occupy increasingly central positions and appear more "hub-like". Additionally, we show that the community structure of long-distance connections spans multiple topological levels and differs from the community structure detected in networks that include both short-range and long-distance connections. In summary, these findings highlight the complex relationship between the brain's physical layout and its functional architecture. The results presented here inform future analyses of community structure and network hubs in health, across development, and in the case of neuropsychiatric disorders.

1. Introduction

Cognitive and psychological processes are underpinned by the coordinated activity of spatially distributed brain areas (Park and Friston, 2013). This coordination pattern can be estimated from observed brain activity and quantified as the statistical dependence of brain regions' activity on one another (Bressler and Menon, 2010). The set of all such measurements can be modeled as a functional network and analyzed using graph theoretic methods (Bullmore and Sporns, 2009; Rubinov and Sporns, 2010).

Analysis of functional networks has revealed a number of key features of brain organization. Among the most salient are the brain's modular structure (Bertolero et al., 2015; Power et al., 2011) and the presence of hub regions – brain areas whose connections span modular boundaries (Power et al., 2013; Gordon et al., 2018). Both of these features can be interpreted in the context of brain function: modules reflect units for performing specialized information processing while hubs reflect the integration of that information from one module to another (van den Heuvel and Sporns, 2013; Sporns and Betzel, 2016).

In general, the organization of functional networks (including hubs and modules) is guided and constrained by many factors. One important factor is the brain's underlying anatomical network of white-matter fiber tracts (Hagmann et al., 2008; Messé et al., 2014; Honey et al., 2009). This anatomical network plays an important role in shaping activity across the brain (Avena-Koenigsberger et al., 2018; Harush and Barzel, 2017) and is, itself, subject to strong metabolic and spatial constraints (Betzel and Bassett, 2018; Stiso and Bassett, 2018; Samu et al., 2014). These constraints effectively place soft limits on the possible number, length, and volume of structural connections (Sherbondy et al., 2009).

The mapping of structural connectivity (SC) to functional

* Corresponding author. Department of Psychological and Brain Sciences, Indiana University, Bloomington, IN, 47405, USA.
E-mail address: rbetzel@indiana.edu (R.F. Betzel).

https://doi.org/10.1016/j.neuroimage.2020.116612
Received 16 November 2019; Accepted 4 February 2020
Available online 17 February 2020

connectivity (FC) is complex (Honey et al., 2009; Goñi et al., 2014; Becker et al., 2018; Betzel et al., 2017a) and constraints on wiring-cost propagate to the level of FC, leading to gradients of distance-dependent inter-areal correlations wherein activity recorded from nearby brain areas tends to be more strongly correlated than that of distant areas (Power et al., 2011; Huntenburg et al., 2017).

How do we disambiguate patterns of FC that arise out of functional necessity from those that arise as a consequence of space? One possibility is to emphasize long-distance FC while discounting short-range FC. Whereas short-range correlations are often directly supported by underlying anatomical connectivity, long-range correlations exist in the absence of such support (Ercsey-Ravasz et al., 2013; Goñi et al., 2014; Hagmann et al., 2008; Honey et al., 2009; Hermundstad et al., 2013). This observation suggests that, without strong structural support, long-range correlations may emerge as a consequence of a different mechanism, motivating studying them further.

The principal aim of this study was to better characterize long-distance functional connectivity and to understand its contribution to the community structure and hub distribution of functional networks. To accomplish this goal, we developed a modeling framework that enabled us to generate synthetic regional time series whose correlation structure exhibited a prescribed distance-dependence (Betzel et al., 2017b). While these synthetic networks exhibited typical patterns of short-range connectivity, they lacked the long-distance correlations that are also observed in functional networks. To shift focus onto those long-distance connections, we subtracted the elements of synthetic matrices from the corresponding elements in the observed functional connectivity matrix. The resulting network contained correlations among different brain regions that were stronger than expected, given the distance between those regions.

Surprisingly, we found that synthetic networks exhibited strong functional connections, both within and between well-characterized canonical brain systems. Next, we show that, after correcting for space, the participation coefficients of brain areas within primary sensory systems (somatomotor and visual) increase, suggesting that they may perform increasingly "hub-like" functional roles based on long-distance connectivity. We then use a data-driven approach for defining communities both with and without a distance correction. Overall, we find that the identified communities are similar across methods, with subtle differences in primary sensory systems but also higher-order cognitive systems, including salience and dorsal attention networks. In summary, these findings present a complex portrait of the relationship between space and functional connectivity. These results inform future studies of brain network communities and hubs, and may further clarify the role of functional connectivity in health, development, and disease.

2. Results

In this paper, we analyze the organization of long-distance functional connections, the results of which are presented in the following subsections. First, in the section **Modeling FC distance dependence**, we explain the basic features of our model and the procedure used to fit the model to observed data. In the next section, **Comparison with cognitive systems**, we introduce the distance-corrected FC matrix, focusing on where it differs from the observed FC matrix. We also show that, given a set of canonical cognitive systems, distance-corrected functional connectivity exhibits subtle, yet systematic, differences in hub locations compared to observed FC. Next, in the section **Incorporating distance-dependence into community detection tools**, we use the distance-corrected functional connectivity matrix as input to a community detection algorithm. With this algorithm, we detect communities in both distance-corrected and observed functional connectivity, and we compare the outputs. Finally, using detected communities, we describe variations in hub organization as a function of community size, reporting four distinct spatial patterns.

2.1. Modeling FC distance dependence

In order to study long-distance functional connectivity, we first needed a method for generating synthetic functional connectivity with a prescribed distance dependence. In addition, we wished to ensure that the resulting synthetic functional connectivity matrix was admissible as a correlation matrix, being positive semidefinite and satisfying transitive relationships. Briefly, our strategy involved generating synthetic regional fMRI BOLD time series using phase-randomization procedures (Fig. 1a*i*). Because phase randomization was performed separately for every brain region, the resulting time series were uncorrelated, on average. To introduce spatial correlations, we defined a new time series for each region as a weighted sum of all other regional time series (Fig. 1a*ii*). Here, the weights were defined to be inversely proportional to the Euclidean distance between pairs of brain regions, so that nearby regions contributed more than distance regions. As a result, the magnitude of inter-regional correlations decreased monotonically as a function of distance (Fig. 1a*iii*). The rate of this decrease was modulated by a single parameter (Fig. 1b and c) and fit to observed data (Fig. 1d). The model is described in greater detail in **Materials and Methods**.

Our approach is similar, in spirit, to previous methods for generating distance-dependent correlation matrices using rational quadratic functions (Bellec et al., 2006), which have proven useful in geospatial statistics (Cressie, 1992). Our approach, however, operates directly on time series whereas the approach of Bellec et al. (2006) and others is model-based. Both approaches generate positive-definite matrices with distance-dependent elements. Throughout this section, we use the synthetic matrices generated by this model as a sort of null condition that allows us to identify a set of spatially unexpected features (Zalesky et al., 2012).

2.2. Comparison with cognitive systems

Functional connectivity can be used to map the brain's organization at the level of systems (Power et al., 2011; Gordon et al., 2014). Analyses of this type generate cortex-wide maps in which brain areas or parcels are assigned to one or another system. These systems, in turn, are often interpreted in the context of brain and cognitive function; for example, some are thought to comprise collections of brain areas that support somatomotor function or for enacting cognitive control. Importantly, in conjunction with network measurements like participation coefficient, these systems have also been used to detect and classify hub areas based on whether an area's connections are distributed across many systems (hub) or concentrated within an area's own system (non-hub) (Power et al., 2013; Gordon et al., 2018; Guimera and Amaral, 2005). Here, we compared observed patterns of functional connectivity with those generated by the spatial model in order to gain insight into the contribution of long-distance connections to the brain's system-level organization and hub structure (Schaefer et al., 2017).

The analyses in this section focused on three inter-dependent connectivity matrices: the observed pattern of functional connectivity, $FC^{observed}$ (Fig. 2a); the synthetic patterns of connectivity generated by the spatial model, $FC^{spatial}$ (Fig. 2b); and the distance-corrected matrix of functional connections, $FC^{corrected}$ (Fig. 2c), which was calculated as the element-wise difference of the observed and spatial matrices, $\left(FC^{observed} - FC^{spatial}\right)$. As expected, when we reordered the $FC^{observed}$ by system, we found that systems were cohesive with strong intra-system correlations (Fig. 2b). When we plotted $FC^{spatial}$, we found that connections within many of the systems were much weaker in comparison (for example, the control networks Conta and Contb). On the other hand, we were surprised to find that a number of systems maintained their cohesiveness despite the fact that their connections reflect a spatial wiring rule rather than relevance to a cognitive or psychological process. The somatomotor and visual systems, for instance, as well as Contc, a subcomponent of the control network, were dominated by strong short-

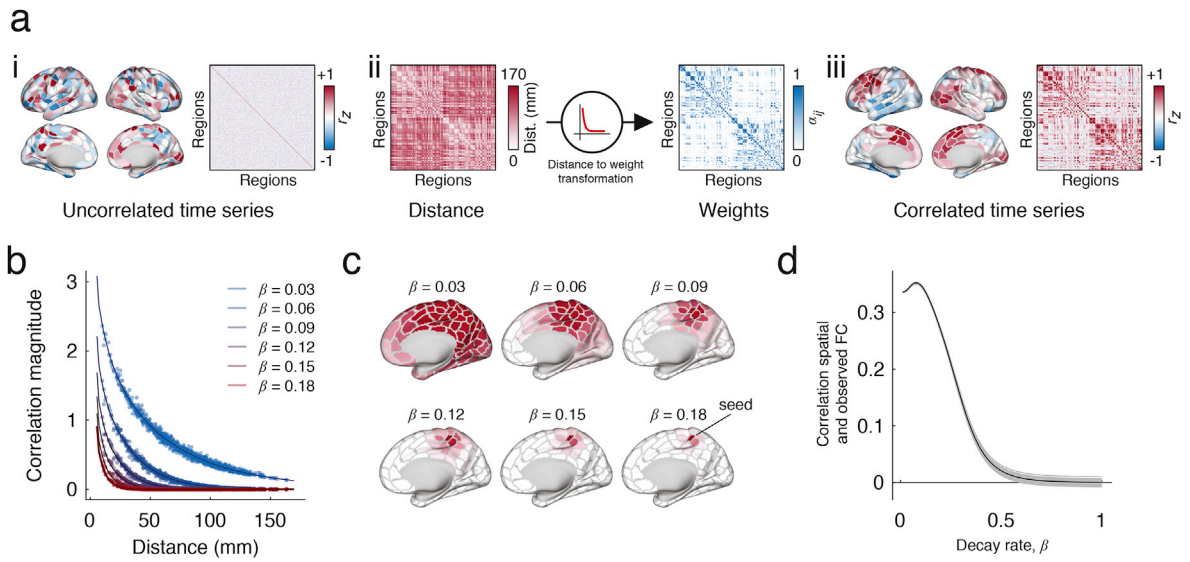

Fig. 1. Procedure for constructing matrices with distance-dependent FC. (*a*) *i*: The procedure begins by introducing a random phase to the observed fMRI BOLD time series. This introduction is performed independently for each brain area, resulting in an uncorrelated surrogate time series. *ii*: Next, we generate a new surrogate time series for each brain area as the linear combination of all other time series. The weighted contribution of brain area *j*'s time series to that of area *i* depends on the distance between those two areas in three-dimensional Euclidean space, D_{ij}. Specifically, this distance-to-weight transformation is modeled as a decaying exponential, $w_{ij} = e^{-\beta D_{ij}}$, where β controls the decay rate. *iii*: This process results in spatially correlated time series. (*b*) The value of β controls the rate of the exponential decay and therefore parameterizes the extent to which time series exhibit more or less spatial correlation. For example, large values of β yield areal time series that are correlated with only their nearby neighbors; smaller values of β yield spatial correlations with much wider neighborhoods. (*c*) Examples of seed-based functional connectivity as we vary the value of β. (*d*) To select the value of β, we compare the similarity of the observed and spatially constrained FC patterns. The optimal value of β is the one that maximizes the correspondence between those matrices.

range connectivity. In Fig. 2c, we show the effect of correcting for these distance effects, noting the now-attenuated connection weights within visual, motor, and control networks (see black arrows).

The observation of commonalities and differences between $FC^{observed}$ and $FC^{spatial}$ has implications for our understanding of brain function. In particular, it suggests that some network features may be driven differentially by short-range or long-distance connections. Here, we focus on the network property of "participation coefficient," a local measure typically interpreted as an index of a region's "hubness". To identify areas whose observed participation coefficient may be driven predominantly by short-range connectivity, we computed each brain area's signed participation coefficient (Guimera and Amaral, 2005) using the function participation_coef_sign.m in the Brain Connectivity Toolbox (https://sites.google.com/site/bctnet/) (Rubinov and Sporns, 2010) with respect to the system assignments reported in Schaefer et al. (2017) (Fig. 3a and b).

We note that, in general, the signed participation coefficient can be calculated based on how either positive or negative connections are distributed across systems. In the main text, we report participation derived using positive connections only. Our rationale for doing so stems from our interpretation of FC and the manner in which modules (and brain systems) are typically defined. Generally, stronger (positive) correlations are interpreted as evidence that two brain regions are functionally related to one another. Modules, then, are groups of regions that are mutually correlated, suggesting that they are collectively engaged in similar processes. In fact, it is this criterion – mutually positively correlated brain regions – that we generally use to define modules. Anti-correlations (negative correlations) are often thresholded away and, if they are retained in an analysis, tend to fall between modules. Again, this reflects the intuition that within-module connections should be mostly positive, reflecting the fact that modules are groups of brain regions that perform similar functions. The participation coefficient is a way of

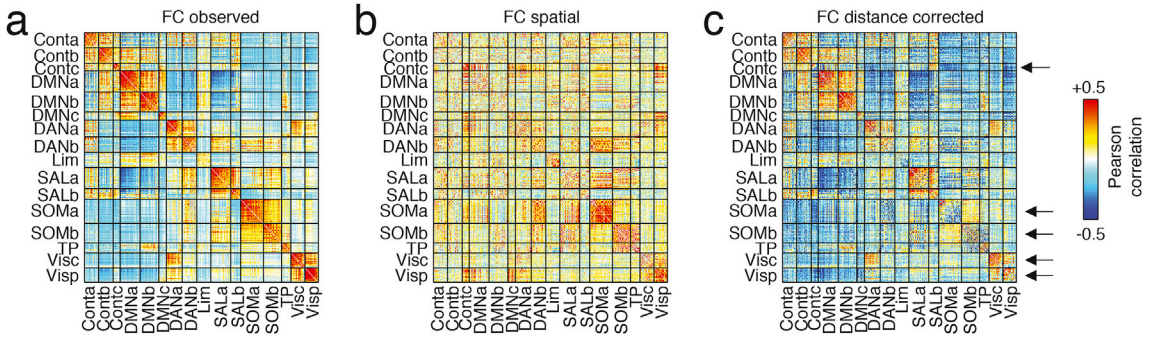

Fig. 2. Differences in correlation structure. (*a*) The original (uncorrected) inter-regional correlation matrix ordered by cognitive system. (*b*) The correlation matrix obtained from the optimal spatial null model. (*c*) We correct for space-induced inter-regional correlation structure by subtracting the spatial null model matrix from the original matrix. Here, the arrows are used to draw attention to salient changes. The top arrow, for instance, shows that after correcting for distance, regions within the "Contc" system become weakly connected to each other. Similarly, in the original network, the correlation magnitude within somatomotor and visual systems are among the strongest across the brain. As with the control network component, these systems exhibit marked reductions in their internal connection strength following correction.

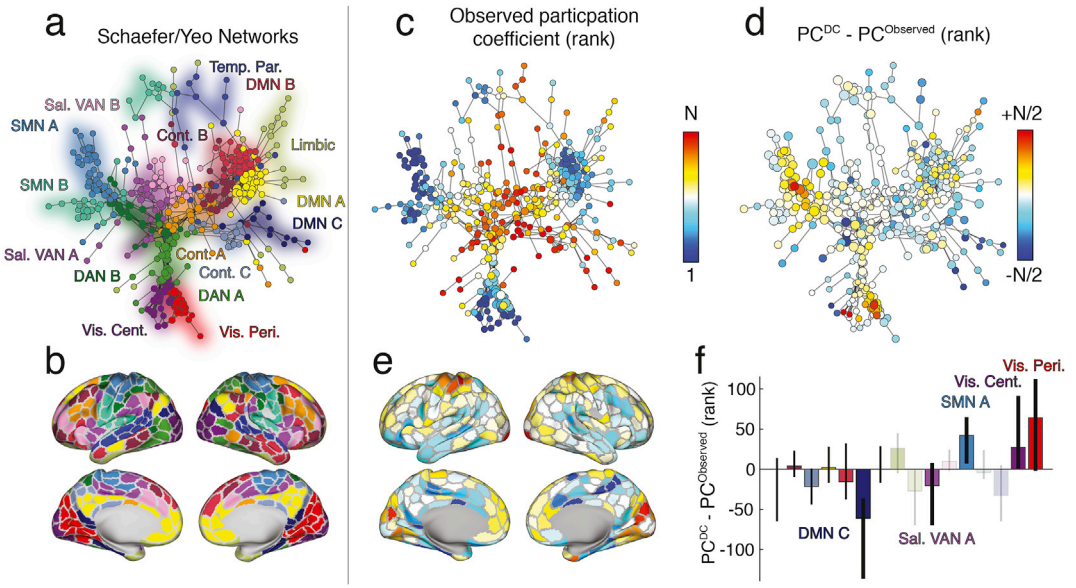

Fig. 3. Effect of distance correction on canonical brain systems and hubness. (*a*) A spring-embedded layout of minimum spanning tree for the original network with no distance correction. Each node corresponds to a brain region, and colors indicate the system to which that region is assigned. (*b*) A surface representation of system labels from panel *a*. (*c*) Similar to panel *a* except color now indicates nodes' ranked participation coefficients calculated using the original network and with respect to the canonically defined brain systems. (*d*) The difference in ranked participation coefficient after correcting for distance. (*e*) Participation coefficient differences projected onto the cortical surface. (*f*) Mean difference in participation coefficient aggregated by system. Opaque and labeled systems are those whose mean difference exceeded chance levels (false discovery rate controlled at 5%).

identifying nodes that are positively correlated with their own module, but also maintain positive correlations with regions in other modules (Guimera and Amaral, 2005). This is thought to reflect the polyfunctionality of certain brain regions. While it makes sense to calculate participation coefficient based on positive correlations to other modules, it makes much less sense to do so based on how a region's negative correlations are distributed over other modules. In summary, we calculate participation coefficient based on positive correlations only. For completeness, however, we repeat our analysis using participation coefficients calculated using negative connections (see Fig. S1).

We repeated this procedure for both the observed (Fig. 3c) and distance-corrected FC matrices. Next, to reduce the effect of confounds, we ranked participation coefficients and computed the difference in rank for each brain area (Fig. 3d and e). The aim of the rank transformation was to reduce biases that arise from low-level properties of connectivity matrices, for example their total weight, binary density, or connection weight distributions. In the supplement we show raw differences in participation coefficient without undergoing a rank transformation (Fig. S2). These properties are known to artificially inflate or deflate network summary statistics, including participation coefficient (Van Wijk et al., 2010). Here, we attempt to circumvent this issue by not comparing raw participation coefficients, but by comparing their ranks, thereby forcing the participation coefficients to have identical distributions, i.e. $P = \{1, \ldots, 400\}$.

Interestingly, we find that the areas with the greatest increases in participation coefficient are concentrated in visual and motor systems ($p < 0.05$; false discovery rate fixed at 5%), indicating that a greater proportion of connections from these areas now span system boundaries. These differences can be attributed to the fact that in the distance-corrected matrix, the weights of functional connections within somatomotor and visual networks are massively attenuated. That is, those connections are expected under the spatial null model. We also observed that the participation within components of the default mode, salience and ventral attention networks decreased significantly ($p < 0.05$; false discovery rate fixed at 5%). In general, participation coefficient increases as self-connections to a node's own module decrease and inter-modular connections increase and become more diverse. We confirmed that this mechanism was driving the observed change in participation by calculating the difference in distance-corrected FC of each node to its own system minus its connectivity to other systems (Fig. S3. As expected, nodes with the biggest increases in PC after distance corrections were the same nodes whose intra-modular connections decreased at a greater rate than their inter-modular connections.

In typical analyses of functional networks, connections of all lengths are treated equally, making it difficult to parse the unique contributions of long- and short-range connections to any topological feature (Rubinov and Sporns, 2010). Our findings suggest that short-range and long-distance connections make differential contributions to the "hubness" of individual brain regions. Specifically, we find that shifting focus onto long-distance connections results in system-wide increases within participation of primary sensory systems. This observation is counter to the traditional classification of these systems as non-hubs (Power et al., 2013; Gordon et al., 2018), a classification that our findings suggest is likely driven by the strong short-range connectivity among the brain regions that comprise those systems. Notably, our observations are in agreement with tract-tracing studies in animal models that have reported long-distance projections visual and sensorimotor areas (Hooks et al., 2018; Oh et al., 2014). We further note that these reported differences in hubness are general, and appear insensitive to variation in features of processing pipelines, e.g. whether or not to perform global signal regression (Murphy and Fox, 2017) (See. Fig. S4). Collectively, our findings suggest an alternative and distance-dependent interpretation of brain areas' functional roles within the broader context of the network.

2.3. *Incorporating distance-dependence into community detection tools*

In the previous section, we treated the system labels (Schaefer et al., 2017) though they are equivalent to communities. While this approach is useful, communities can also be defined by data-driven methods. Here, we use the community detection heuristic "modularity maximization" to identify and compare communities in the observed and distance-corrected functional connectivity matrices (Newman and Girvan, 2004).

Specifically, we used a variant of modularity maximization known to

work well with correlation matrices (Bazzi et al., 2016) and that we have applied to functional connectivity matrices in previous papers (Betzel et al., 2016a, 2017a; Betzel and Bassett, 2018). To ensure that comparisons between the two matrices are as appropriate as possible, we guided the modularity maximization algorithm so that it detected a prescribed number of communities, k (by selectively varying its resolution parameter, γ). This additional constraint guaranteed that every comparison between the original and distance-corrected networks was made using partitions that resulted in an equal number of communities (Figure, 4a).

Each comparison entailed several steps. First, we computed the pairwise similarity of the partitions using the z-score of the Rand index (Traud et al., 2011) (see **Materials and Methods**). In general, larger z-scores indicated higher levels of similarity. We used this measure to compare partitions detected using the original and distance-corrected matrices (Fig. 4b). In general, we found that partitions detected using the two techniques were similar.

Nonetheless, there were subtle differences. To better characterize these differences, we identified the numbers of communities present for which similarity was lowest. We found that these minima occurred when the number of communities were $k = 16$ and $k = 31$ (Fig. 4c). To identify the community features that were driving this dissimilarity, we computed the difference in community co-assignment matrices. Briefly, a co-assignment matrix (alternatively referred to as an "agreement", "consensus", or "allegiance" matrix) counts the fraction of times that a pair of nodes were co-assigned to the same community given an ensemble of partitions. For non-deterministic community detection methods like modularity maximization, the co-assignment matrix serves as a pseudo-continuous way of partitioning the network into communities. Comparing co-assignment matrices allows us to identify differences in communities between the two matrices.

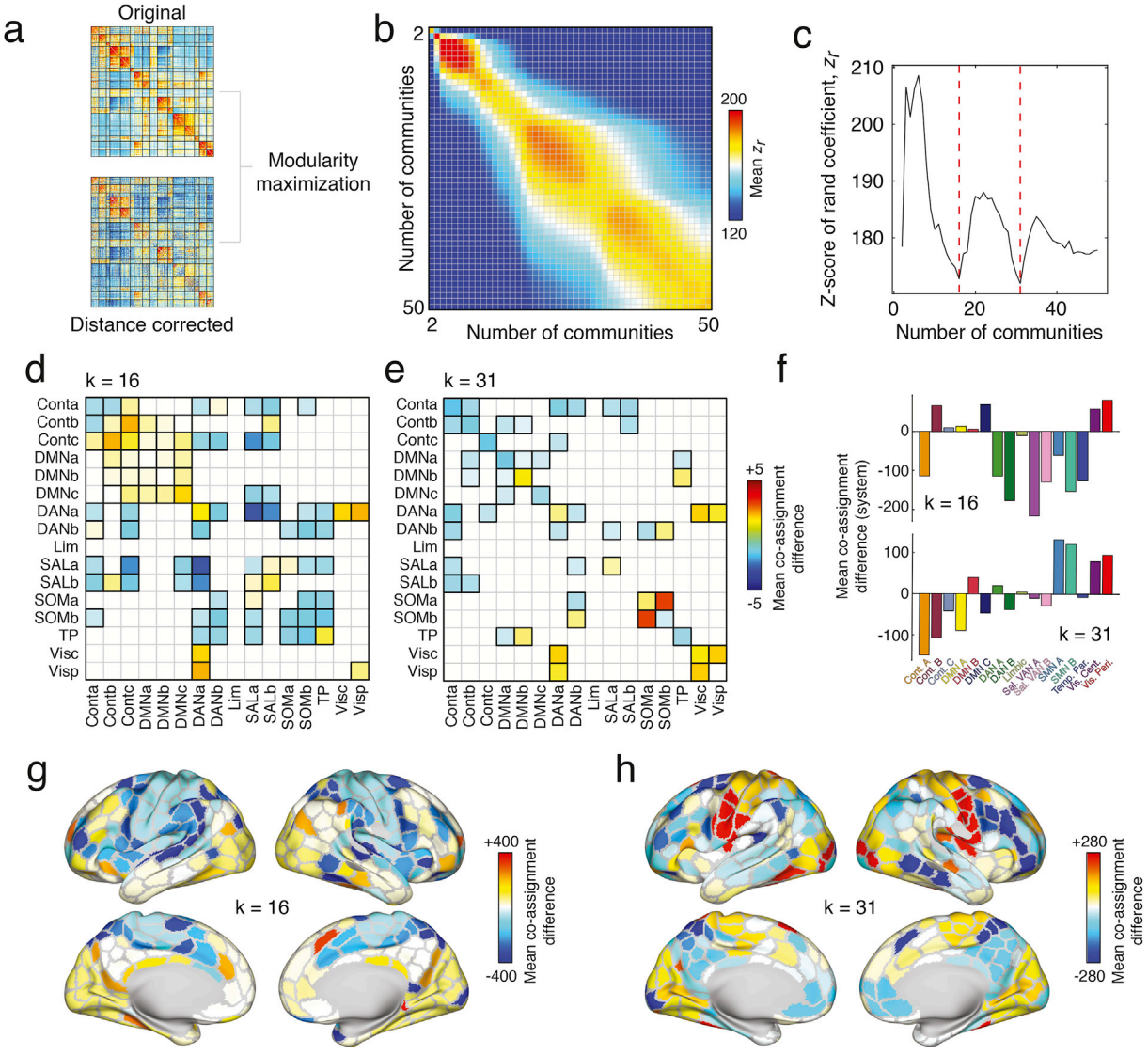

Fig. 4. Data-driven estimation and comparison of community structure. (*a*) We used modularity maximization to detect communities in the original and distance-corrected FC matrices. (*b*) We arranged community partitions based on the number of detected communities and compared them using the z-score of the Rand index. Here, we show the mean similarity as a function of the number of communities. (*c*) To narrow our comparisons, we focused on partitions of the brain into 16 and 31 communities, which corresponded to local minima along the diagonal of the matrix shown in panel *b*. Panels *d* and *e* show statistically significant differences in mean module co-assignment. Here and in all subsequent plots, the differences in co-assignment values reflect distance-corrected minus original. Thus, warm colors indicate nodes/systems that are more likely to be co-assigned after correcting for distance; cool colors reflect greater co-assignment in the original matrix than in the distance-corrected matrix. Pairs of systems that survive statistical comparisons have black borders. To better identify those regions and systems whose community co-assignment differed the greatest, we calculated the mean co-assignment difference for every brain region with all other brain regions. In panel *f* we further average those mean differences by system for the $k = 16$ (*top*) and $k = 31$ (*bottom*) partitions. In panels *g* and *h*, we show mean differences plotted on the cortical surface.

To provide better context, we aggregated differences in co-assignment probability by brain systems and compared mean co-assignment differences to those obtained using a permutation-based null model in which the number and size of communities were retained but where nodes were otherwise assigned to communities randomly ($p < 0.05$; false discovery rate fixed at 5%) (Fig. 4d and e). In both cases, we observed many subtle yet significant differences. Among the most salient when $k = 16$ were decreases in the co-assignment probabilities of brain areas in the salience network with those in the dorsal attention system and increased co-assignment probability of control network sub-components with one another. In other words, regions associated with these respective networks were more likely to be observed in the same community after correcting for distance than in the original network. Similarly, when $k = 31$, we found increased co-clustering probability within the broader visual and somatomotor systems.

We summarized these results further, calculating the average co-assignment difference for each brain region and subsequently averaging these values for every system (Fig. 4f,g,h). As expected, when $k = 16$, the systems with the greatest co-assignment decreases were concentrated in the salience and dorsal attention systems (Fig. 4f, top), whereas with $k = 31$, the greatest biggest changes occurred within somatomotor and visual networks (Fig. 4f, bottom).

Collectively, these results suggest that differences in observed and distance-corrected functional connectivity are subtle, as evidenced by the high z-score Rand indices. However, these differences are also systematic and emphasized within and between particular brain systems. Moreover, these differences span multiple organizational scales (Betzel and Bassett, 2017). As in the previous section, these findings suggest that accounting for spatially-driven patterns of FC and focusing on long-distance patterns of inter-areal coupling reveals novel network features; in this case, manifesting in the form of novel community structure.

2.4. Multi-scale changes in participation coefficient and distinct contributions from somatomotor and visual systems

In the previous two sections, we demonstrated that by comparing observed and spatially constrained patterns of functional connectivity, we were able to tease apart features of networks that are driven differentially by short-range or long-distance connections. Our results also

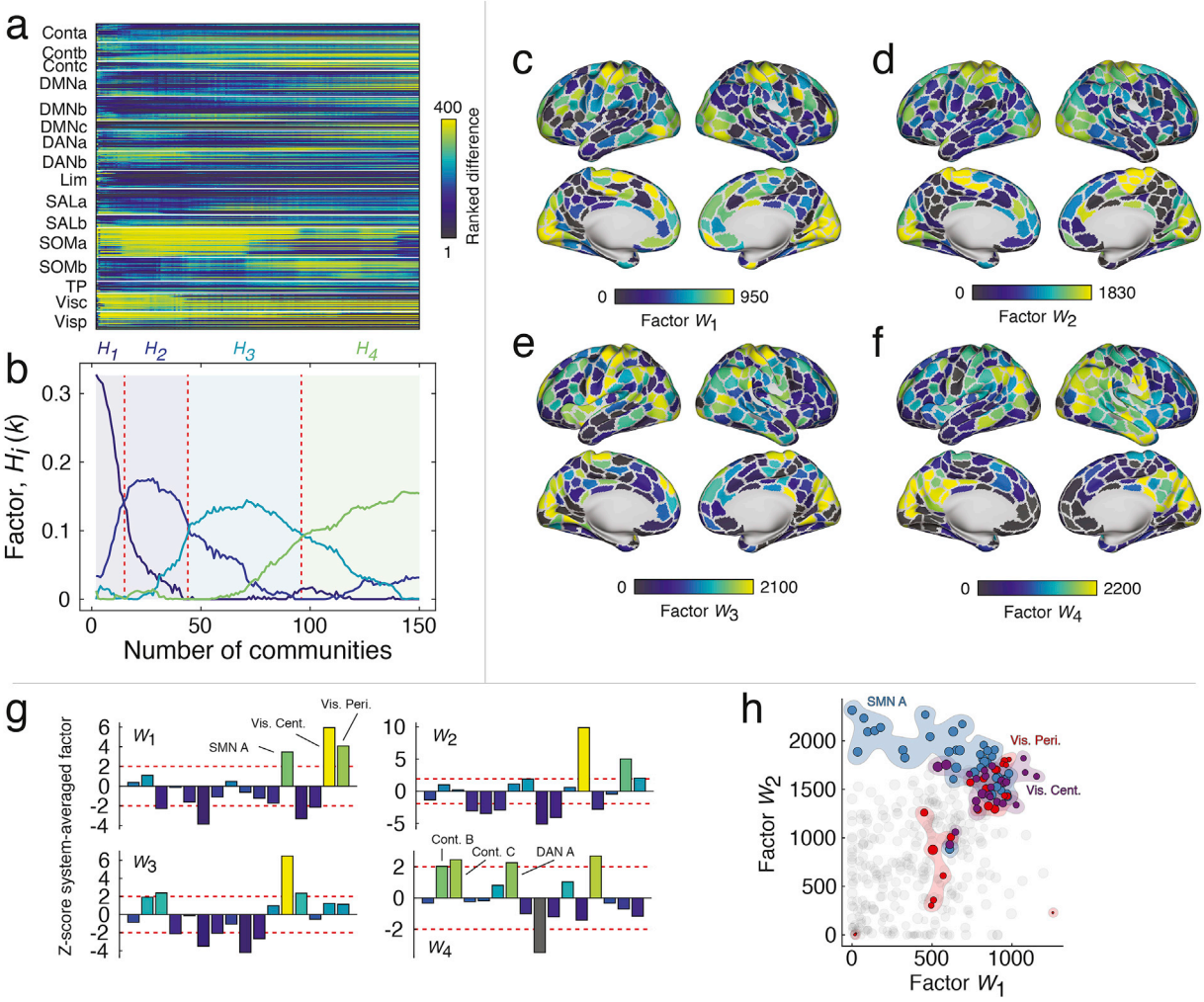

Fig. 5. Results of non-negative matrix factorization. (*a*) Ranked differences in participation coefficients for all brain regions and with the number of communities ranging from 2 to 150. This matrix served as input to the NMF algorithm. (*b*) NMF identified four factors that approximately reconstructed the original data. Broadly, these factors were associated with different topological regimes corresponding to different numbers of communities. In panels *c–f* we show the factors mapped onto the cortical surface. Note that the first three factors emphasize participation coefficient differences in motor and visual systems while the fourth factor highlights widespread, multi-system differences. (*g*) We show system-averaged and z-scored differences in participation coefficient. Note that the first three factors all emphasize motor and visual systems but in different proportions. (*h*) Scatterplot of first two factors against one another. Note that somatomotor and visual areas tend to display the largest values in general. However, note also that those areas deviate from the diagonal, indicating that differences in these systems are emphasized differentially by the two factors and at different topological scales.

suggested that differences in community structure were manifest at multiple topological scales. This observation is consistent with the idea that brain networks exhibit neuroscientifically relevant features at and across different levels of organization (Betzel and Bassett, 2017). Here, we pursue this idea further and characterize multi-scale structure of brain areas' participation coefficients and the network's hub distribution.

To explore multi-scale hub structure, we first calculated the difference in participation coefficient estimated using the distance-corrected and distance-uncorrected networks. We performed this analysis separately for each brain region and, because we were interested in relative and not absolute changes in participation coefficient, we rank-transformed these values. We then repeated this procedure while varying the number of communities from 2 to 150 (Fig. 5a). Then, we used non-negative matrix factorization (NMF) to generate low-rank approximations of the participation coefficient differences. We compared how well the reconstructed data fit the observed data and found that increasing the number of dimensions beyond four led to little improvement in the overall fit. We repeated the algorithm 100 times and identified, from those repetitions, the group of factors that best reconstructed the original data.

Analyzing those four factors further, we found that their expression varied more or less smoothly as a function of the number of communities (Fig. 5b). Broadly speaking, the first three factors were similar to one another, in that they emphasized increased participation coefficient within visual and somatomotor areas. However, the extent to which those systems and respective subsystems was expressed varied (Fig. 5c–e). For instance, the first factor (W_1) exhibited differences in the participation coefficient of visual areas and peaked earlier, in terms community number, than factors W_2 and W_3 (Fig. 5g). Those factors, on the other hand, peaked later and emphasized the differences in somatomotor participation coefficient. These differences are made more pointed when we directly compare W_1 with W_2 in a scatterplot (Fig. 5h). We find, in both cases, that visual and motor areas are among the strongest values, but that the somatomotor system (SMN A) falls to the left of the main diagonal (stronger in W_2) while the visual system (VisCent) falls to the right of the main diagonal (stronger in W_1). The fourth factor, on the other hand, peaked the latest and exhibited neither motor nor visual systems, but more spatially diffuse differences among control and dorsal attention systems (Fig. 5f and g).

The import of these findings spans several domains. First, the results suggest that space-corrected hub structure varies, as a function of the number of detected communities, albeit subtly. This observation agrees with recent multi-scale accounts of brain network structure that have suggested that the brain exhibits unique and functionally relevant organizational features at multiple topological scales (Betzel and Bassett, 2017). Multi-scale and hierarchical organization is critical for complex systems, as it engenders robustness to perturbations and separation of dynamical timescales (Bar-Yam, 2004), properties that are essential for embodied nervous systems that interact with variable environments.

3. Discussion

In this report, we analyzed the contributions of long-distance connectivity to the community and hub structure of functional brain networks. To do this, we developed a surrogate-based method that generates synthetic networks lacking long-distance correlations but preserving short-range connectivity. We found that even these null networks exhibited neuroscientifically interesting structure, including strong correlations within primary sensory systems, such as visual and somatomotor areas, as well as sub-components of higher-order cognitive systems, such control networks. These observations suggested that connections of different lengths contribute to shape the overall character of the network.

Next, to better understand those distinct contributions, we suppressed the contributions from short-range connections by constructing a "distance-corrected" connectivity matrix in which we simply subtracted the short-range synthetic network from the observed. The resulting network expressed long-distance connections but effectively suppressed those made between proximal brain areas. We compared the features of the distance-corrected network to those of the observed network and found that the participation coefficient of visual and somatomotor regions increased in the distance-corrected network, suggesting that the long-distance connectivity patterns of these brain areas leave those systems increasingly well-situated for integrating information across communities. We also found evidence that the community structures of the two networks differed across multiple topological scales, confirming further that long-distance and short-range connections uniquely shape the organization of functional networks. In summary, our work shows that the weights of functional connections exhibit a complicated relationship with space and distance, but also presents a flexible corrective strategy for teasing apart the contributions of spatial sources to functional connectivity. Our approach outlines a procedure that enables future studies to conduct a more nuanced analysis of functional networks in both health and disease.

3.1. Spatial constraints and brain connectivity

Here, we present a careful analysis of functional networks in which we discount the effect of short-range connections. Why bother doing so? What can we learn about brain organization and function by studying connections of different lengths? The primary justification for focusing on longer connections is that they entail greater costs than short connections (all other things equal) and that their mere existence suggests functional relevance (Laughlin and Sejnowski, 2003; Stiso and Bassett, 2018). This is certainly true in the case of structural and anatomical connections, where the metabolic and material costs of forming and maintaining axonal projections or fiber tracts grow as a function of their length and diameter (Samu et al., 2014; Roberts et al., 2016; Betzel et al., 2016b). It is also likely true in the case of functional connections, which are the focus of this study and which require energy to maintain correlated activity over long distances (Hasenstaub et al., 2010). In this light, the analyses presented can be viewed as effectively shifting focus onto the more costly features of functional networks and ones that, we argue, are of greater relevance to the overall network function. This argument stems from the observation that a particular brain function could be instantiated equally well by networks comprised of short-range or long-distance connections, then we would expect that evolution would favor the architecture comprised of shorter and less-costly connections. The fact that long-distance connections are nonetheless present in both anatomical and functional networks (Samu et al., 2014; Bellec et al., 2006), suggests that whatever brain functions those connections help support, those functions could not easily be performed by networks composed of only short-range connections.

We acknowledge that in focusing on long and costly functional connections, we necessarily overlook network features that are driven by short-range connectivity. This is not to say that short connections are irrelevant to network function. Short-range connections are generally among the strongest in functional networks, and they factor disproportionately in the weighted shortest path structure of anatomical networks (Betzel and Bassett, 2018), and enhancing the cohesiveness of communities (Sporns and Betzel, 2016). Accordingly, we view short-range and long-distance connections as complementary, with each delivering unique insights into the organization and behavior of functional networks.

In addition to characterizing the organization of long-distance functional connections, our study also contributes some useful methodology. An important component of any network neuroscience study is the comparison of some measurement made on the observed network with a null distribution of the same measure made on an ensemble of appropriately constructed random networks. Because the randomized networks tend to preserve only low-level features of the observed network, e.g. average binary density, degree sequence, etc., this hypothesis testing framework allows us to identify higher-level features of the observed

network that are not easily attributable to random fluctuations (Fosdick et al., 2018). Increasingly, it is becoming understood that the traditional random network models can be too liberal for many of the hypothesis testings (Henderson and Robinson, 2013; Klimm et al., 2014; Rubinov, 2016; Gollo et al., 2018). That is, though they preserve degree (in un-weighted network) or strength (in weighted network) sequences, they also fail to preserve other key attributes of real-world brain networks, including wiring cost, or violate mathematical relationships when applied to correlation matrices (Zalesky et al., 2012). These failures can result in mischaracterizations of networks, which identify features that act as "spandrels" and emerge as a result of relatively benign processes (Rubinov, 2016). The spatial null model we use here addresses some of these concerns, as it generates admissible correlation matrices and allows the user to flexibly model spatial relationships. In future work, similar null models could be used both to identify novel network features and better clarify the relationship of known features with psychological phenomena and brain function.

3.2. Increased participation coefficient in primary sensory regions

One of the most salient findings we report is the increased participation coefficient of brain regions comprising the visual and somatomotor systems. The conventional interpretation of high-participation nodes is that they serve as network "hubs" (Power et al., 2013; Bertolero et al., 2017); their connections form bridges across multiple sub-systems, which engenders or reflects the polyfunctionality of those regions (Guimera and Amaral, 2005; van den Heuvel and Sporns, 2013). In past studies, somatomotor and visual areas were generally reported among the least hub-like parts of the brain; regions in those systems made strong connections within their respective communities but weak extra-community connections (Bertolero et al., 2017; Power et al., 2013; Gordon et al., 2018). Our findings, on the other hand, suggest that the low levels of "hubness" in those regions is a direct consequence of their strong short-range connectivity and that, in terms of their longer connections, visual and motor systems can be regarded as much more hub-like. These observations suggest expanded functional roles for these systems, which are traditionally associated with uni-modal information processing. Future work should investigate this question more directly.

It is essential to note that the relationship between a region's "hubness" and its connection's lengths is, in general, more complicated. Here, we actively discount contributions made by short-range connectivity to each region's hubness, focusing instead on the contributions of longer-range connections, which may be associated with greater material and metabolic cost (Stiso and Bassett, 2018). However, many studies have shown that the brain networks of different species adopt near-optimal spatial configurations in terms of wiring cost (Kaiser and Hilgetag, 2004; Cherniak, 1994). This leaves open the possibility that, over the course of evolution, pressure to reduce wiring cost could lead to migration of neuronal populations, so that the length (cost) of functionally important long-distance connections are reduced. Future work using non-human connectivity data could be undertaken to investigate support for this hypothesis (Van den Heuvel et al., 2016).

3.3. A less severe approach to control for spatial artifacts

Occasionally spatial relationships have been discussed in the context of FC, most often with respect to the origins of short-range FC. Many influential studies, for instance, regard short-range FC as having artifactual origins and, as a way of addressing such artifacts, simply discard all FC between regions separated by distances less than some threshold, e.g. 20 mm (Power et al., 2011). While this strategy is effective in reducing the number of false-positives (artifactually strong short-range correlations), it may inadvertently discard true-positives and does so in a binary way – connections are either retained or discarded, with no middle ground. The strategy we propose here, on the other hand, offers a graded and more systematic way of taking into account the spatial proximity of connections in functional connectivity analysis. Specifically, the severity with which we discount a connection's observed weight decays monotonically with the distance between nodes. So the closer two nodes are to one another, the greater the extent to which they are discounted. In this sense, our strategy may prove more beneficial, in that the continuous discounting of connections does not throw away connectivity information; the short-range connections can still contribute to estimates of community structure or participation, but with less overall influence.

3.4. Limitations

Though this study makes several important contributions, it also has a number of limitations. First, this study focuses on group-averaged FC rather than FC of single subjects. While this strategy facilitates computation (we only have to fit the models to a single connectivity matrix), the lack of single-subject analyses means that we may fail to appreciate the individual variability in weight-distance dependencies (Finn et al., 2015) and also run the risk of characterizing patterns in the group matrix that are not representative of any typical subject (Simpson et al., 2012). Indeed, future applied studies are needed to determine how results reported here map onto individual subjects and how those mappings are related to inter-individual variability in subjects' performances on psychometric and cognitive tests.

Another challenge involves processing decisions made as part of modeling distance-dependent FC. Essentially, we treat the observed FC as though it were made up of three components: "extra-spatial" + "spatial" + "error" FC. Our aim was, as best as possible, to subtract away the spatial component, leaving only the true FC and error terms. The challenge, however, is that we do not know the actual forms of *any* of the three components nor do we know the function by which they are intermixed. Here, we assume that the spatially-driven FC decays exponentially with distance and that by 60 mm its effect is small (Bellec et al., 2006). We also assume that the spatial component enters linearly, so that its effect can be subtracted out. While these assumptions were made with practical considerations in mind, such as model parsimony and computational complexity, future work should investigate and test these assumptions systematically and explicitly.

The aim of this study was to present a principled method for isolating connections whose weights were stronger than expected, given their Euclidean distance. We accomplished this by developing a simple, spatial null model for FC in which connection weight decayed monotonically and exponentially as a function of distance. While this model is computationally tractable is neurophysiologically inspired, effectively capturing the well-documented spatial dependence of observed structural and functional connectivity (Betzel and Bassett, 2018; Stiso and Bassett, 2018; Samu et al., 2014; Ercsey-Ravasz et al., 2013; Bellec et al., 2006; Roberts et al., 2016; Betzel et al., 2016b; Kaiser and Hilgetag, 2004; Margulies et al., 2016), it nonetheless lacks precise neurophysiological mechanisms.

Although, our model provides insight into the contributions of long-distance FC to graph-theoretic measures of information integration and segregation – participation coefficient and modularity, respectively – it could, provide further and potentially deeper insight by incorporating neurophysiological detail into a biophysical model. Neural mass models (NMMs), for instance, are generative models of population-level neural activity and have been used in the past in conjunction with estimates of structural connectivity to produce synthetic fMRI BOLD time series and FC (Woolrich and Stephan, 2013). NMMs include parameters that represent biophysical attributes of nervous systems, such as ion channel properties, propagation delays, and firing rates of inhibitory and excitatory neuronal populations (Honey et al., 2009; Heitmann et al., 2018). Future studies should focus on strategies for generating spatially-constrained FC based on the output of NMMs constrained by estimates of SC.

Finally, here we have used Euclidean distance to obtain the weighted contribution of different brain areas. However, previous studies

(Oosterhof et al., 2011) suggest that using Euclidean distance could potentially reduce the spatial selectivity, meaning that functionally different regions could be selected by voxel selection methods that depend on Euclidean distance. Therefore, other distance measures such as geodesic distance that respect the curvature of the cortex during calculations should be studied and its performance compared to Euclidean distance.

4. Materials and methods

4.1. Human connectome dataset

In this study, we aimed to characterize the relationship between space and resting state FC. To address this aim, we leveraged data from the Human Connectome Project (HCP), a multi-site consortia that collected extensive MRI, behavioral, and demographic data from a large cohort of subjects (>1000) (Van Essen et al., 2013). As part of the HCP protocol, subjects underwent two separate resting state scans along with seven task fMRI scans. All functional connectivity data analyzed in this report came from these scans and was part of the HCP S1200 release (Van Essen et al., 2013). Subjects that completed both resting-state scans and all task scans were analyzed. We utilized a cortical parcellation that maximizes the similarity of functional connectivity within each parcel ($N = 400$ parcels) (Schaefer et al., 2017).

We processed ICA-FIX data provided by the HCP, which used ICA to remove nuisance and motion signals (Glasser et al., 2013). In addition, the 12 detrended motion estimates provided by the Human Connectome Project were regressed out from the time series, the mean global signal was removed, and the time series was bandpass filtered from 0.009 to 0.08 Hz.

For all scans, the MSMAII registration was used, and the mean time series of vertices on the cortical surface (fsL32K) in each parcel was calculated. These time series were z-scored and concatenated across all subjects. A group representative functional connectivity matrix was then calculated as the pairwise Pearson correlation (subsequently Fisher z-transformed) between concatenated node time series. We denote this matrix as A and whose element A_{ij} refers to the Fisher-transformed correlation between regions i and j.

4.2. Modeling distance dependence

Our goal was to understand the role of spatial relationships in shaping whole-brain FC. To investigate this question, we constructed a distance-based null model. We reasoned that this model should have the following properties: 1) FC should decay monotonically with distance, so that proximal brain areas are more strongly correlated than distant brain areas; 2) the connectivity matrix must be admissible as a correlation matrix (Zalesky et al., 2012). These requirements are in contrast to current null models for FC, in which binarized connections are rewired while preserving degree – an operation that can result in edge configurations that violate transitive relationships associated with the correlation metric (Bellec et al., 2006).

There are many ways of realizing such a model, though here we focused on a single possibility based on surrogate time series analysis. Suppose $x_i = [x_i(t)]$ is the observed activity recorded from brain area $i \in N$. We could generate a surrogate time series with the same power spectrum by taking the discrete Fourier transform of x_i, adding or subtracting random amounts of phase to each frequency bin, and performing an inverse Fourier transform. We denote the resulting time series as x_i'. We note that the phase-randomization surrogate procedure was always carried out at the level of individual subjects; all surrogate time series were subsequently concatenated.

If we performed this operation independently and for each brain area, the resulting inter-areal correlations would be weak, and the full matrix would exhibit no structure. To induce spatial dependencies, we generate for each brain area another time series, $x_i^{spatial}$, that is the linear combination of every other regions' time series, but where the mixing coefficients are distance-dependent:

$$x_i^d = \sum_j \alpha_{ij} x_j', \tag{1}$$

where α_{ij} is defined according to the function $f(D_{ij}, \beta)$. Here, D_{ij} is the Euclidean distance between nodes i and j, and β is the parameter that controls the decay rate of FC with distance. In general, we define this function in any way, but for practical reasons and to maintain consistency with previous work, we defined it to be the exponential: $f(D_{ij}, \beta) = \exp(-\beta \cdot D_{ij})$ (Kaiser and Hilgetag, 2004; Betzel et al., 2017b).

Fitting this model amounted to choosing the β parameter that optimizes some objective function. Here, we used the bisection method to maximize the correlation of the observed FC matrix, A, with the distance-dependent FC matrix, $A^{spatial}$. We defined model fitness as the average fitness over 50 independently generated surrogate time series (optimal fitness of $r = 0.35$ at $\beta = 0.078$).

5. Modularity maximization

It is generally understood that brain networks can be decomposed into clusters defined based on nodes' connectivity patterns. These clusters, also called communities or modules, are typically unknown ahead of time and estimated using data-driven approaches. Of so-called community detection methods, modularity maximization remains one of the most widely used. Modularity maximization operates on a simple principle: compare the connectivity patterns we observe with those we would expect by chance. Communities are defined as groups of nodes more strongly connected to one another than expected. This intuition can be formalized by the modularity heuristic. If $B_{ij} = A_{ij} - P_{ij}$ represents the difference in weight of the observed and expected connection between node i and j, then we can define the following quality function:

$$Q = \sum_{ij} B_{ij} \delta(\sigma_i \sigma_j). \tag{2}$$

In this expression, $\delta(\cdot, \cdot)$ is the Kronecker delta function, whose value is 1 if its arguments are equal and 0 otherwise. Here, its arguments are the σ_i and σ_j, which denote the community assignments of nodes i and j. As a result of the delta function, the only elements B_{ij} that contribute to the summation are those that fall within communities.

The value of Q can be used to rate the quality of a proposed community partition. Alternatively, an optimal community structure can be uncovered by assigning nodes to the communities that optimize Q. This optimization procedure is computationally intractable, though the optimal solution can be approximated using several heuristics, the most popular of which is the so-called "Louvain algorithm": a non-deterministic and agglomerative method that generally performs well on most benchmarking tests.

Here, we use a modularity framework that has been extended in several important ways. First, we focus on a "multi-scale" version in which a structural resolution parameter, γ, is introduced to the modularity matrix: $B_{ij} = A_{ij} - \gamma P_{ij}$. The value of γ can be tuned to smaller or larger values to, effectively, uncover communities of correspondingly larger or smaller size, respectively. Second, we define the expected weight of connections to be $P_{ij} = 1$ for all $\{i,j\}$. This particular null model has proven to be compatible with correlation matrices and results in an intuitive definition of communities as groups of nodes whose average internal density exceeds a value of γ. To detect the community structure of observed FC (uncorrected for distance), we optimized the following multi-scale modularity index:

$$Q(\gamma) = \sum_{ij} [A_{ij} - \gamma] \delta(\sigma_i, \sigma_j). \tag{3}$$

We note that this modularity function is compatible with signed and weighted networks and has been used successfully in previous studies to uncover the system-level organization of functional brain networks (Betzel and Bassett, 2018; Betzel et al., 2019). Of course, there exists other modularity functions that are also applicable to signed and weighted networks. These other methods treat positive and negative correlations separately (Rubinov and Sporns, 2011; Gómez et al., 2009) and are susceptible to biases introduced by a resolution limit, which effectively blinds those methods from detecting communities below a characteristic scale (Fortunato and Barthelemy, 2007).

5.1. Distance-dependent modularity maximization

We optimized a similar modularity index to detect communities for distance-corrected FC by defining the modularity matrix: $B_{ij}^{corrected} = [A_{ij} - A_{ij}^{sptl}] - \gamma$. The distance-corrected modularity can then be expressed as:

$$Q(\gamma) = \sum_{ij} [A_{ij} - A_{ij}^{sptl} - \gamma]\delta(\sigma_i, \sigma_j). \quad (4)$$

We optimized both the original and distance-dependent modularity using a generalized version of the Louvain algorithm. Typically, as part of multi-scale community detection, the value of γ is either systematically or randomly sampled over some predefined range. Here, we aimed to compare the multi-scale community structure of distance-corrected and uncorrected FC. To ensure that the comparison was as fair as possible, e.g., not comparing a partition of the network into two communities with another that divides the network into twenty communities, we used an adaptive algorithm to sample partitions of both distance-corrected and uncorrected FC into the same number of communities.

To do so, we used a two-step adaptive algorithm. First, we coarsely sampled 1001 different γ values over the range of $\gamma = -0.2$ to $\gamma = 0.7$, which encompasses the range of neuroscientifically interesting partitions. We optimized $Q(\gamma)$ for each network and for each value of γ and calculated the number of communities in the resulting partition. Using this approach, we obtained a rough mapping of γ to the number of communities. This mapping allowed us to select a number of communities, e.g., $k = 14$, and specify a range of γ values for which we could reasonably expect to obtain 14 communities. Finally, we varied the value of k from 2 to 150, sampling γ from restricted ranges until, for each value of k, we sampled 250. We repeated this procedure for both the uncorrected and distance-corrected FC matrices, resulting in two sets of 37,500 partitions in total.

We note that all subsequent analyses were carried out on ensembles of detected partitions. That is, for a given number of communities, k, we characterized the statistical properties of the 250 partitions that resulted in k communities. Alternatively, we could have estimated an "average" or consensus partition at each value of k (or for windows of k) (Lancichinetti and Fortunato, 2012). This approach can be advantageous if the aim is of an analysis is to condense the variability within a partition ensemble into a point estimate, e.g. for parcellation generation (Eickhoff et al., 2018). However, it is well-known that the landscape of partitions generated by modularity maximization and other community detection methods is "nearly degenerate" (Good et al., 2010). This means that the algorithms will generate many dissimilar partitions that are approximately equally modular (the severity of this degeneracy grows exponentially with the number of nodes). To avoid the possibility of generating a consensus partition that is not representative of the partition ensemble, we focused instead on the statistical properties of the ensemble.

5.2. Z-scored rand index for partition similarity

We used the z-score of the Rand index to measure the similarity of partitions detected using the uncorrected and distance-corrected FC matrices. This measure is similar to the traditional Rand index but corrects for biases induced by the number and size of the communities in the partitions being compared. For two partitions, X and Y, we measure their similarity as:

$$Z_{XY} = \frac{1}{\sigma_{w_{XY}}} w_{XY} - \frac{W_X W_Y}{W}. \quad (5)$$

Here, W is the total number of node pairs in the network, W_X and W_Y are the number of pairs in the same modules in partitions X and Y, respectively, w_{XY} is the number of pairs assigned to the same module in *both* X and Y, and $\sigma_{w_{XY}}$ is the standard deviation of w_{XY}. The value of Z_{XY} can be interpreted as how great, beyond chance, is the similarity of partitions X and Y.

5.3. Participation coefficient

Using the detected communities and based on FC, we can also identify those brain regions whose connections span the boundaries of communities (polyfunctional) and those whose connections are confined, largely, to their own community (unifunctional). To identify these kinds of brain regions, we calculated the network measure *participation coefficient* for each brain region, i, which we denote as P_i:

$$P_i = 1 - \sum_{s=1}^{K} \left(\frac{k_{is}}{k_i}\right)^2. \quad (6)$$

Here, $k_i = \sum_j A_{ij}$ is node i's weighted degree and $k_{is} = \sum_{j \in s} A_{ij}$ is the total weight of node i's connections to module s. Participation coefficients range from 0 to 1, where larger values indicate that connections are evenly spread over modules. Here, because our matrices were signed, we used a modified version of participation coefficient that considers only positive connections. To ensure that comparisons were unbiased by the effect of weight, we rank-transformed brain regions' participation coefficients.

5.4. Non-negative matrix factorization

Non-negative matrix factorization (NMF) is a technique that generates low-rank approximations of a, potentially, high-dimensional dataset, $\mathbf{X} \in \mathbb{R}^{n \times p}$. Briefly, this approach entails identifying matrices $\mathbf{W} \in \mathbb{R}^{n \times k}$ and $\mathbf{H} \in \mathbb{R}^{k \times p}$ such that $\mathbf{W} \times \mathbf{H} \approx \mathbf{X}$ and subject to the constraint that all elements of $\mathbf{W}$ and $\mathbf{H}$ are non-negative. Here, we used NMF to decompose brain-wide participation coefficients as the number of communities varied from 2 to 150. Thus the dataset had dimensions $\mathbf{X} \in \mathbb{R}^{400 \times 149}$. The MATLAB implementation of NMF uses the non-deterministic alternating least squares algorithm to determine $\mathbf{W}$ and $\mathbf{H}$. Consequently, we repeated the algorithm 100 times with different initial conditions as we varied the rank from $k = 2$ to $k = 20$. We observed that the root mean square of the residual (a measure of fitness) decreased sharply until $k = 4$, suggesting that the original dataset could be reasonably approximated using four dimensions.

Data and code availability statement

All fMRI data are freely available as part of the Human Connectome Project (https://www.humanconnectome.org). Code for generating spatial surrogate time series is freely available (https://www.brainnetworkslab.com/s/spatialFC.zip). All other code is available upon reasonable request.

Acknowledgements

This research was supported by Indiana University Office of the Vice President for Research Emerging Area of Research Initiative, Learning: Brains, Machines and Children (FZE and RFB). DSB acknowledges

support from the John D. and Catherine T. MacArthur Foundation, the Alfred P. Sloan Foundation, the Paul G. Allen Foundation, the Army Research Laboratory through contract number W911NF-10-2-0022, the Army Research Office through contract numbers W911NF-14-1-0679 and W911NF-16-1-0474, the National Institutes of Health (2-R01-DC-009209-11, 1R01HD086888-01, R01-MH107235, R01-MH107703, R01MH109520, 1R01NS099348 and R21-M MH-106799), the Office of Naval Research, and the National Science Foundation (BCS-1441502, CAREER PHY-1554488, BCS-1631550, and CNS-1626008). The content is solely the responsibility of the authors and does not necessarily represent the official views of any of the funding agencies.

Appendix A. Supplementary data

Supplementary data to this article can be found online at https://doi.org/10.1016/j.neuroimage.2020.116612.

References

Avena-Koenigsberger, A., Misic, B., Sporns, O., 2018. Nat. Rev. Neurosci. 19, 17.
Bar-Yam, Y., 2004. Complexity 9, 37.
Bazzi, M., Porter, M.A., Williams, S., McDonald, M., Fenn, D.J., Howison, S.D., 2016. Multiscale Model. Simul. 14, 1.
Becker, C.O., Pequito, S., Pappas, G.J., Miller, M.B., Grafton, S.T., Bassett, D.S., Preciado, V.M., 2018. Sci. Rep. 8, 1411.
Bellec, P., Perlbarg, V., Jbabdi, S., Pélégrini-Issac, M., Anton, J.-L., Doyon, J., Benali, H., 2006. Neuroimage 29, 1231.
Bertolero, M.A., Yeo, B.T., D'Esposito, M., 2015. Proc. Natl. Acad. Sci. Unit. States Am. 112, E6798.
Bertolero, M., Yeo, B., D'Esposito, M., 2017. Nat. Commun. 8, 1277.
Betzel, R.F., Bassett, D.S., 2017. Neuroimage 160, 73.
Betzel, R.F., Bassett, D.S., 2018. Proc. Natl. Acad. Sci. Unit. States Am., 201720186
Betzel, R.F., Fukushima, M., He, Y., Zuo, X.-N., Sporns, O., 2016a. Neuroimage 127, 287.
Betzel, R.F., Avena-Koenigsberger, A., Goñi, J., He, Y., De Reus, M.A., Griffa, A., Vértes, P.E., Mišic, B., Thiran, J.-P., Hagmann, P., et al., 2016b. Neuroimage 124, 1054.
R. F. Betzel, J. D. Medaglia, A. E. Kahn, J. Soffer, D. R. Schonhaut, and D. S. Bassett, arXiv preprint arXiv:1706.06088 (2017a)
Betzel, R.F., Medaglia, J.D., Papadopoulos, L., Baum, G.L., Gur, R., Gur, R., Roalf, D., Satterthwaite, T.D., Bassett, D.S., 2017b. Netw. Neurosci. 1, 42.
Betzel, R.F., Bertolero, M.A., Gordon, E.M., Gratton, C., Dosenbach, N.U., Bassett, D.S., 2019. Neuroimage 202, 115990.
Bressler, S.L., Menon, V., 2010. Trends Cognit. Sci. 14, 277.
Bullmore, E., Sporns, O., 2009. Nat. Rev. Neurosci. 10, 186.
Cherniak, C., 1994. J. Neurosci. 14, 2418.
Cressie, N., 1992. Terra. Nova 4, 613.
Eickhoff, S.B., Yeo, B.T., Genon, S., 2018. Nat. Rev. Neurosci. 19, 672.
Ercsey-Ravasz, M., Markov, N.T., Lamy, C., Van Essen, D.C., Knoblauch, K., Toroczkai, Z., Kennedy, H., 2013. Neuron 80, 184.
Finn, E.S., Shen, X., Scheinost, D., Rosenberg, M.D., Huang, J., Chun, M.M., Papademetris, X., Constable, R.T., 2015. Nat. Neurosci. 18, 1664.
Fortunato, S., Barthelemy, M., 2007. Proc. Natl. Acad. Sci. Unit. States Am. 104, 36.
Fosdick, B.K., Larremore, D.B., Nishimura, J., Ugander, J., 2018. SIAM Rev. 60, 315.
Glasser, M.F., Sotiropoulos, S.N., Wilson, J.A., Coalson, T.S., Fischl, B., Andersson, J.L., Xu, J., Jbabdi, S., Webster, M., Polimeni, J.R., et al., 2013. Neuroimage 80, 105.
Gollo, L.L., Roberts, J.A., Cropley, V.L., Di Biase, M.A., Pantelis, C., Zalesky, A., Breakspear, M., 2018. Nat. Neurosci. 21, 1107.
Gómez, S., Jensen, P., Arenas, A., 2009. Phys. Rev. 80, 016114.
Goñi, J., van den Heuvel, M.P., Avena-Koenigsberger, A., de Mendizabal, N.V., Betzel, R.F., Griffa, A., Hagmann, P., Corominas-Murtra, B., Thiran, J.-P., Sporns, O., 2014. Proc. Natl. Acad. Sci. Unit. States Am. 111, 833.
Good, B.H., De Montjoye, Y.-A., Clauset, A., 2010. Phys. Rev. 81, 046106.
Gordon, E.M., Laumann, T.O., Adeyemo, B., Huckins, J.F., Kelley, W.M., Petersen, S.E., 2014. Cerebr. Cortex 26, 288.
Gordon, E.M., Lynch, C.J., Gratton, C., Laumann, T.O., Gilmore, A.W., Greene, D.J., Ortega, M., Nguyen, A.L., Schlaggar, B.L., Petersen, S.E., et al., 2018. Cell Rep. 24, 1687.
Guimera, R., Amaral, L.A.N., 2005. Nature 433, 895.
Hagmann, P., Cammoun, L., Gigandet, X., Meuli, R., Honey, C.J., Wedeen, V.J., Sporns, O., 2008. PLoS Biol. 6, e159.
Harush, U., Barzel, B., 2017. Nat. Commun. 8, 2181.
Hasenstaub, A., Otte, S., Callaway, E., Sejnowski, T.J., 2010. Proc. Natl. Acad. Sci. Unit. States Am. 107, 12329.
Heitmann, S., Aburn, M.J., Breakspear, M., 2018. Neurocomputing 315, 82.
Henderson, J.A., Robinson, P.A., 2013. Brain Connect. 3, 423.
Hermundstad, A.M., Bassett, D.S., Brown, K.S., Aminoff, E.M., Clewett, D., Freeman, S., Frithsen, A., Johnson, A., Tipper, C.M., Miller, M.B., et al., 2013. Proc. Natl. Acad. Sci. Unit. States Am. 110, 6169.
Honey, C., Sporns, O., Cammoun, L., Gigandet, X., Thiran, J.-P., Meuli, R., Hagmann, P., 2009. Proc. Natl. Acad. Sci. Unit. States Am. 106, 2035.
Hooks, B.M., Papale, A.E., Paletzki, R.F., Feroze, M.W., Eastwood, B.S., Couey, J.J., Winnubst, J., Chandrashekar, J., Gerfen, C.R., 2018. Nat. Commun. 9, 3549.
Huntenburg, J.M., Bazin, P.-L., Margulies, D.S., 2017. Trends in Cognitive Sciences.
Kaiser, M., Hilgetag, C.C., 2004. Phys. Rev. 69, 036103.
Klimm, F., Bassett, D.S., Carlson, J.M., Mucha, P.J., 2014. PLoS Comput. Biol. 10, e1003491.
Lancichinetti, A., Fortunato, S., 2012. Sci. Rep. 2, 336.
Laughlin, S.B., Sejnowski, T.J., 2003. Science 301, 1870.
Margulies, D.S., Ghosh, S.S., Goulas, A., Falkiewicz, M., Huntenburg, J.M., Langs, G., Bezgin, G., Eickhoff, S.B., Castellanos, F.X., Petrides, M., et al., 2016. Proc. Natl. Acad. Sci. Unit. States Am. 113, 12574.
Messé, A., Rudrauf, D., Benali, H., Marrelec, G., 2014. PLoS Comput. Biol. 10, e1003530.
Murphy, K., Fox, M.D., 2017. Neuroimage 154, 169.
Newman, M.E., Girvan, M., 2004. Phys. Rev. E 69, 026113.
Oh, S.W., Harris, J.A., Ng, L., Winslow, B., Cain, N., Mihalas, S., Wang, Q., Lau, C., Kuan, L., Henry, A.M., et al., 2014. Nature 508, 207.
Oosterhof, N.N., Wiestler, T., Downing, P.E., Diedrichsen, J., 2011. Neuroimage 56, 593.
Park, H.-J., Friston, K., 2013. Science 342, 1238411.
Power, J.D., Cohen, A.L., Nelson, S.M., Wig, G.S., Barnes, K.A., Church, J.A., Vogel, A.C., Laumann, T.O., Miezin, F.M., Schlaggar, B.L., et al., 2011. Neuron 72, 665.
Power, J.D., Schlaggar, B.L., Lessov-Schlaggar, C.N., Petersen, S.E., 2013. Neuron 79, 798.
Roberts, J.A., Perry, A., Lord, A.R., Roberts, G., Mitchell, P.B., Smith, R.E., Calamante, F., Breakspear, M., 2016. Neuroimage 124, 379.
Rubinov, M., 2016. Nat. Commun. 7, 13812.
Rubinov, M., Sporns, O., 2010. Neuroimage 52, 1059.
Rubinov, M., Sporns, O., 2011. Neuroimage 56, 2068.
Samu, D., Seth, A.K., Nowotny, T., 2014. PLoS Comput. Biol. 10, e1003557.
Schaefer, A., Kong, R., Gordon, E.M., Laumann, T.O., Zuo, X.-N., Holmes, A.J., Eickhoff, S.B., Yeo, B.T., 2017. Cerebr. Cortex 1.
Sherbondy, A.J., Dougherty, R.F., Ananthanarayanan, R., Modha, D.S., Wandell, B.A., 2009. In: International Conference on Medical Image Computing and Computer-Assisted Intervention. Springer, pp. 861–868.
Simpson, S.L., Moussa, M.N., Laurienti, P.J., 2012. Neuroimage 60, 1117.
Sporns, O., Betzel, R.F., 2016. Annu. Rev. Psychol. 67, 613.
J. Stiso and D. Bassett, arXiv preprint arXiv:1807.04691 (2018)
Traud, A.L., Kelsic, E.D., Mucha, P.J., Porter, M.A., 2011. SIAM Rev. 53, 526.
van den Heuvel, M.P., Sporns, O., 2013. Trends Cognit. Sci. 17, 683.
Van den Heuvel, M.P., Bullmore, E.T., Sporns, O., 2016. Trends Cognit. Sci. 20, 345.
Van Essen, D.C., Smith, S.M., Barch, D.M., Behrens, T.E., Yacoub, E., Ugurbil, K., Consortium, W.-M.H., et al., 2013. Neuroimage 80, 62.
Van Wijk, B.C., Stam, C.J., Daffertshofer, A., 2010. PloS One 5, e13701.
Woolrich, M.W., Stephan, K.E., 2013. Neuroimage 80, 330.
Zalesky, A., Fornito, A., Bullmore, E., 2012. Neuroimage 60, 2096.